PCCP

Accepted Manuscript

ROYAL SOCIETY OF CHEMISTRY

www.rsc.org/pccp

Physical Chemistry Chemical Physics

ARTICLE

Revealing the working mechanism of polymer photodetectors with ultra-high external quantum efficiency

Received 00th January 20xx,
Accepted 00th January 20xx

DOI: 10.1039/x0xx00000x

www.rsc.org/

Lingliang Li,[a] Fujun Zhang,*[,a] Wenbin Wang,[a] Yanjun Fang,[b] Jinsong Huang†[,b]

We report polymer photodetectors (PPDs) with evident photomultiplication (PM) phenomenon, based on sandwich structure ITO/PEDOT:PSS/P3HT:$PC_{71}BM$(100:1)/Al. The similar device structure has been latterly reported in our previous work, showing great potential as a new type of high performance PPDs. However, we found more interesting new phenomenons from these PPDs. Solid evidences are provided to prove the existence of photogenerated electron transport in the almost hole-only active layer under applied bias. The transport of photogenerated electrons leads to the electron accumulation near the Al electrode and the electron redistribution, which strongly affect the EQE spectral shape and transient response of the PPDs. Our conclusion is further confirmed by confirmatory devices with structure of Al(1)/P3HT:$PC_{71}BM$(100:1)/Al(2). EQE spectra and transient J_{ph} of the confirmatory devices well accord with our speculation. This discovery may provide a new insight to increase the response speed of PM type PPDs by adjusting the photogenerated electron distribution in the active layer. Considering that the PM type PPDs have much higher EQE than the traditional organic photodetectors, the improvement may further extend its potential application with low cost.

Introduction

Organic photodetectors are receiving an ever growing attention due to their ease of fabrication, wide selection of materials and large-area processing capability.[1] There is growing interest in the development of colour selective[2-4], ultraviolet[5], near-infrared[6], and panchromatic[7] organic photodetectors. Most of organic photodetectors are photodiode type with photocurrent originated from the collection of photogenerated charge carriers.[8, 9] Low back ground noise and fast response of photodiode type organic photodetectors are beneficial to practical applications such as optical communications, remote control and image sensing.[10-12] The pre-amplifiers are needed to read the weak photocurrent of photodetectors with low external quantum efficiency (EQE) values under weak light condition [13], which may bring new source of noise and make the system more expensive. Therefore, the potential application of photodiode type organic photodetectors may be limited due to the relatively low EQE values (usually lower than 100%). The most important challenge of organic photodetectors is to obtain ultra-high EQE under weak light conditions. [14, 15]

Photomultiplication (PM) phenomenon represents a large number of charge carrier flowing across a photodetector per incident photon, resulting in EQE values (i.e. photoconductive gain factors or multiplication rates) higher than 100%.[16, 17] It is rather difficult to realize PM phenomenon in organic photodetectors based on the mechanism of photomultiplier tubes or avalanche photodiodes due to the relatively high binding energy of organic semiconductors.[18] However, alternative strategies have been successfully realized for obtaining PM phenomenon in organic photodetectors: co-planar structure with or without trap-assisted injection (including photoconductors and phototransistors) [19-21], sandwich structure with trap-assisted charge carrier tunneling injection[18], and sandwich structure with blocking-layer-assisted charge carrier tunneling injection[22]. The mechanism of PM phenomenon in organic photodetectors is that the photogenerated holes or electrons are trapped or blocked in the active layers, while opposite charge carries continually pass through the active layers and are collected by the corresponding electrode. Chuang et al. reported highly sensitive polymer photodetectors (P3HT:$PC_{61}BM$:Ir-125:Q-switch1 =1:1:0.5:0.5 wt %) with PM phenomenon, which is attributed to the unbalanced carrier transport in the active layers with dye materials as electron traps.[23] Chen reported organic-inorganic hybrid photodetectors based on composites of P3HT:$PC_{61}BM$:CdTe (1:1:3.1 wt %) with PM phenomenon under a low reverse bias of 4.5 V, which is also attributed to the unbalanced carrier transport in the active layers with CdTe nanoparticles as electron traps[24]. Guo reported PM type hybrid photodetectors based on polymer/inorganic nanocomposite of PVK:ZnO and P3HT:ZnO (both 1:3 wt %) as the active layer.[25]

[a] Key Laboratory of Luminescence and Optical Information, Ministry of Education, Beijing Jiaotong University, Beijing 100044, People's Republic of China
[b] Department of Mechanical and Materials Engineering and Nebraska Center for Materials and Nanoscience, University of Nebraska–Lincoln, Lincoln, Nebraska 68588-0656, USA
* E-mail: fjzhang@bjtu.edu.cn
† E-mail: jhuang2@unl.edu

Electronic Supplementary Information (ESI) available: [detailed optical field distribution, EQE spectra, transmittance spectrum, transient J_{ph} curves and the spectrum of the light source used in this work]. See DOI: 10.1039/x0xx00000x

The hybrid photodetectors exhibit high EQE values and rather low dark current under -9 V bias for the absence of continuous electron transport channel in the active layers and the rather high Schottky barrier for hole injection. Recently, we successfully fabricated PM type polymer photodetectors (PPDs) using P3HT:$PC_{71}BM$ or P3HT:$PC_{61}BM$ (both 100:1 wt %) as the active layers sandwiched between ITO and Al electrodes, exhibiting EQE values higher than 16,700% or 37,500%,[26, 27] which is among the highest reported values for photodetectors prepared from solely polymer/organic materials. Meanwhile, the detectivity is as high as about 3.5×10^{13} Jones even though our PM type PPDs are without charge blocking layer or any other optimizations. For the active layers with rather low fullerene derivation content, electron and hole injection barrier is ~ 1.7 eV and ~ 0.9 eV from ITO onto the lowest unoccupied molecular orbital (LUMO) of P3HT and from Al onto the highest occupied molecular orbital (HOMO) of P3HT under reverse bias in dark conditions, resulting in a rather low dark current and high detectivity. The small amount of $PC_{71}BM$ or $PC_{61}BM$ will form nano-size aggregations in P3HT matrix, which can be considered as bulk electron traps according to the energy level alignment. This speculation can be further confirmed from the research on polymer solar cells, the optimized donor/acceptor doping weight ratio is about 1:1 to form bicontinuous interpenetrating network for efficient charge carriers transport[28-30]. Up to now, the PM type PPDs based on P3HT:PCBM (100:1) as the active layer have not been commonly approved although the PPDs exhibit rather high EQE values. Therefore, more detailed investigation should be carried out to further clarify the key physical issues in the PM type PPDs.

Experimental

Preparation of the solutions: P3HT (Product No: LT-S909, purchased from Luminescence Technology Corp) and $PC_{71}BM$ (Product No:LT-S923, purchased from Luminescence Technology Corp) were dissolved in 1,2-dichlorobenzene (extra pure, purchased from J&K Scientific Ltd.) to prepare 40 mg ml^{-1} solutions, respectively. Then, the P3HT and $PC_{71}BM$ solutions were blended in volume ratio of 100:1.

Fabrication of the PPDs: ITO glass substrates with a sheet resistance of 15 Ω $square^{-1}$ (purchased from Shenzhen Jinghua Display Co., Ltd.) were pre-cleaned by ultrasonic treatment in detergent, deioned water and ethanol in ultrasonic sequentially. Then, all the substrates were dried by nitrogen-gas and treated by UV-ozone for 10 minutes to increase the work function of ITO substrate. The solution of PEDOT:PSS (Clevios P VP. Al 4083, purchased from Heraeus Precious Metal Gmbh & Co. KG) was spin-coated onto the ITO glass substrates at 5000 round per minute (rpm) for 40 s. The PEDOT:PSS coated ITO glass substrates were baked in air at 120°C. After drying for 10 minutes, the substrates were transferred to a nitrogen-filled glove box. The P3HT:$PC_{71}BM$ blend solution was spin-coated onto the PEDOT:PSS layers at 800 rpm for 30 s to prepare the active layers. The Al electrode of about 100 nm was deposited on the active layers under vacuum (10^{-4} pa) condition. The active area of each PPD is about 3.8 mm^2, which is defined by the vertical overlap of the ITO electrode and the Al electrode.

Fabrication of the confirmatory devices: The Al(1) layers of 20 nm thickness were deposited onto the pre-cleaned glass substrates under vacuum (10^{-4} pa) condition. The P3HT:$PC_{71}BM$ blend solution was spin-coated onto the Al(1) layers at 800 rpm for 30 s to prepare the active layers. Then, the Al(2) layers of about 100 nm were deposited on the active layers under vacuum (10^{-4} pa) condition. The active area is about 2.25 mm^2, which is defined by the vertical overlap of the Al(1) and the Al(2) electrodes.

Measurements: Current densities of PPDs and confirmatory devices were measured using the Keithley 2400 Source Meter. The monochromatic light used in all measurements was provided by a 150 W xenon lamp coupled with a monochromator. Light intensity spectrum of the monochromatic light was measured by a Thorlabs S120VC power meter and is shown in **Fig. S4**. The light-on timing and bias-on timing in transient photocurrent experiment were controlled by electrical shutters and electromagnetic relays, respectively. Absorption and transmittance spectra of films were measured by a Shimadzu UV-3101 PC spectrophotometer. The active layer thickness of PPDs and confirmatory devices was measured by an Ambios technology XP-2 stylus profilometer. The thickness of the Al(1) electrode was monitored by quartz monitor crystals and checked by the Ambios technology XP-2 stylus profilometer.

Calculation: EQE and responsivity (R) of photodetectors are calculated according to the following equations

$$\mathrm{EQE} = \frac{J_{ph}h\nu}{I_{in}e} \quad (1)$$

$$R = \frac{J_{ph}}{I_{in}} \quad (2)$$

Here, J_{ph} is photocurrent density, $h\nu$ is photon energy, I_{in} is incident light intensity and e is absolute value of electron charge.

Based on the assumption that noise-current dominated by shot noise in the dark current, the corresponding detectivity (D^*), which describes the signal-to-noise performances of the photodetectors, can be inferred as [8, 31]:

$$D^* = \frac{R}{\sqrt{2eJ_d}} \quad (3)$$

Here, J_d is dark current density.

Results and discussion

In this work, ultrasensitive PPDs with distinct PM phenomenon were obtained based on P3HT:$PC_{71}BM$ (100:1 wt %) as the active layers. A distinct EQE spectral shape dependence on bias is observed, which may be attributed to the redistribution of photogenerated electrons under different

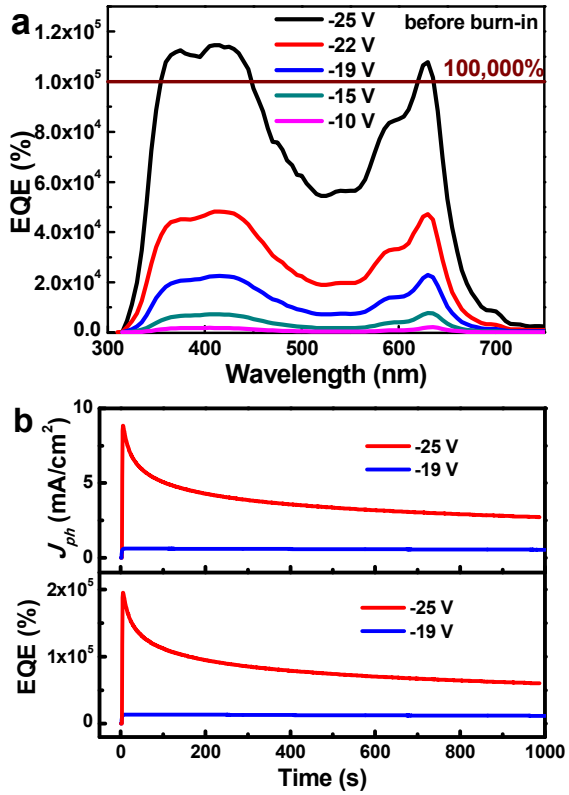

Fig. 1. (a) EQE spectra of PPDs (without burn-in treatment). (b) J_{ph} and EQE value dependence on the burn-in time, the first treatment: under 400 nm light illumination with intensity 14.05 μW/cm^2 and -25 V bias for 1,000 seconds, the second treatment: 400 nm light illumination with intensity 14.05 μW/cm^2 and -19 V bias for another 1,000 seconds.

biases. The redistribution of photogenerated electrons in the active layer can be effectively confirmed from the transient J_{ph} curves under different light illumination and different biases, which may be the main underlying reason for the relatively slow response of PM type PPDs.

The EQE spectra of the PPDs were measured under different biases, as shown in **Fig. 1a**. It is apparent that the EQE values of PPDs are much higher than 100% in the wide spectral range from 350 nm to 750 nm. There is a distinct dip at about 520 nm and two peaks at about 400 nm and 625 nm in the EQE spectra of the PPDs. The maximum EQE values of PPDs at 400 nm and 625 nm arrive to about 112,100% and 107,400% under -25 V bias, respectively. The PM phenomenon is attributed to the trap-assisted hole tunneling injection from Al electrode onto HOMO level of P3HT.[26] For the P3HT:$PC_{71}BM$ blend films with 1 wt % $PC_{71}BM$, $PC_{71}BM$ molecules or aggregations can be considered as electron traps in P3HT matrix due to the relatively high barrier of about 1.3 eV between the LUMO levels of P3HT (-3.0 eV) and $PC_{71}BM$ (-4.3 eV). The trapped electrons in $PC_{71}BM$ near Al electrode can induce the interfacial band bending, resulting in the narrower barrier for the stronger hole tunneling injection. To obtain more solid experimental results to reveal the underlying mechanism of

Table 1: Dark current density (J_d), EQE values, responsivity (R) and detectivity (D^*) of PPDs with or without burn-in treatment

	-19 V (W)	-19 V (W/O)	-25 V (W/O)
J_d (mA/cm^2)	7.5×10^{-3}	1.3×10^{-2}	1.6×10^{-1}
EQE (%)	12,600	21,800	112,100
R (A/W)	40.56	70.26	361.16
D^* (Jones)	2.6×10^{13}	3.5×10^{13}	5.0×10^{13}

The values of EQE, R and D^* were measured under 400 nm light illumination, W: with 2,000 s burn-in treatment, W/O: without burn-in treatment.

the PPDs, all PPDs were pretreated by a burn-in treatment under high bias.

The EQE value as a function of burn-in time is calculated according to the measured J_{ph} as a function of burn-in time, as shown in **Fig. 1b**. All PPDs were illuminated under 400 nm light with an intensity of 14.05 μW/cm^2, the J_{ph} of PPDs were measured under -25 V bias for 1,000 seconds (red curve in **Fig. 1b**) and then under -19 V bias for another 1,000 seconds treatment (blue curve in **Fig. 1b**). It is apparent that the J_{ph} and EQE value of PPDs were sharply decreased at the first 1,000 s burn-in process under -25 V bias and were almost kept as constant during the second 1,000 s burn-in treatment, representing that PPDs arrive to a relatively stable state.

The stable PPDs provide a platform to clarify the underlying mechanism of PM type PPDs. In the following sections, the characterizations on PPDs are based on the devices that have experienced 2,000 s burn-in treatments. The J_d, EQE, R and D^* of PPDs without or with burn-in treatment are summarized in the **Table 1**. The PPDs with burn-in treatments have light-to-dark-current ratio (J_l-J_d ratio) about 77 even under a rather weak incident light intensity 14.05 μW/cm^2 at 400 nm.

The EQE spectra of PPDs were measured under different reverse biases and are shown in **Fig. 2a**. It is apparent that the EQE values are increased along with increase of reverse bias, especially in the dip range from 490 nm to 570 nm. The apparent dip range in the EQE spectra of PPDs well corresponds to the strong absorption range of P3HT, as marked in **Fig. 2a**. To reveal the EQE spectral shape dependence on the reverse bias, all EQE spectra of PPDs under different biases are normalized, as shown in **Fig. 2b**. It is apparent that the dip of EQE spectra becomes shallower along with the increase of reverse bias. It is known that the EQE values of PPDs strongly depend on the hole tunneling injection which is determined by the number of trapped electrons in $PC_{71}BM$ near Al electrode.[26] The variation of EQE spectral shape under different biases indicates that the number of trapped electrons in $PC_{71}BM$ near Al electrode has been changed along with the increase of reverse bias due to the redistribution of photogenerated electrons under bias. To confirm this speculation, the optical field distribution in the PPDs was simulated and is shown in **Fig. S1**. Apparent interference phenomenon can be observed due to the superposition between the incident light and the reflected light from the specular Al electrode in the active layers.[32, 33]

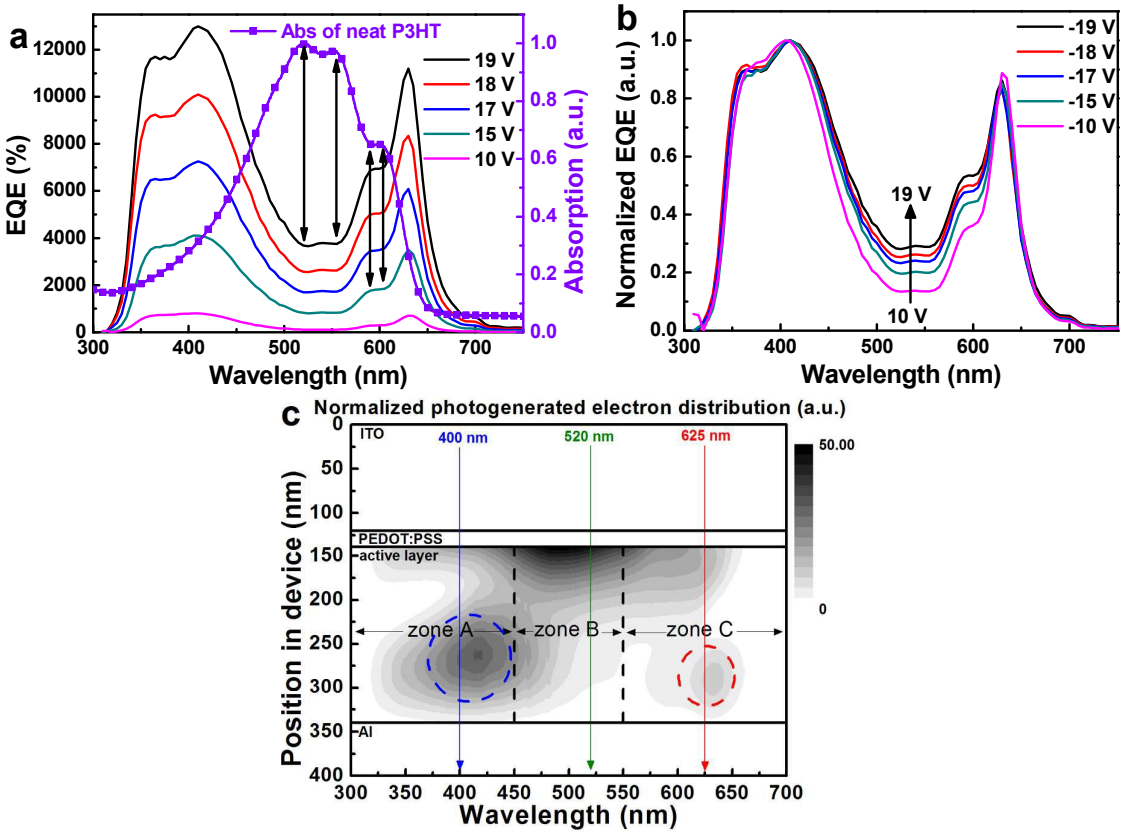

Fig. 2. EQE spectra of the PPDs under different revers biases and the absorption spectrum of neat P3HT films: (a) absolute values; (b) normalized according to the maximum EQE values. (c) The calculated distribution of photogenerated electrons in the active layers (without bias).

Assuming the constant of exciton dissociation coefficient and absorption coefficient in the bulk films due to good miscibility of P3HT and $PC_{71}BM$,[34, 35] the distribution of photogenerated electrons in the active layer (without bias) was calculated according to the optical field distribution and absorption spectrum of P3HT, as shown in **Fig. 2c**. The detailed calculation of the distribution of photogenerated electrons in the active layer is described in the Supporting Information (SI).

For better discussion on distribution of photogenerated electrons in the active layers, we define three zones A (< 450 nm), B (450 to 600 nm) and C (> 600 nm), as marked in **Fig. 2c**. The dark color indicates more photogenerated electrons in the region. It is apparent that much more photogenerated electrons should be trapped in $PC_{71}BM$ near Al electrode in zone A due to the large dark region (marked by a blue imaginary circle), which can well explain the relatively high EQE values in the wide spectra range from 350 nm to 450 nm. For the zone C, there is relatively small and slight dark region in the range from 600 nm to 650 nm (marked by a red imaginary circle), indicating fewer electrons trapped in $PC_{71}BM$ near Al electrode, which also well corresponds to the narrow peak at 625 nm in the EQE spectra of PPDs. For the zones A and C, many photogenerated electrons have been already trapped in $PC_{71}BM$ near Al electrode, those electrons play the key role in assisting hole tunnelling injection from Al electrode onto the HOMO of P3HT. The distribution of photogenerated electrons in zone B is very distinguished from that of zones A and C. Much more photogenerated electrons in zone B are generated near ITO electrode rather than Al electrode due to the strong photon harvesting ability of P3HT in this spectral range. Only very few photons can propagate through the active layer and be reflected by the specular Al electrode, resulting in a rather weak interference in this spectral range. As we can envisage, photogenerated electrons near ITO electrode can be transported toward Al electrode under the electric field induced by reverse bias, leading to the electron accumulation in $PC_{71}BM$ near Al electrode. However, this kind of electron accumulation will be hindered by the electrons already trapped near Al electrode in zone A and zone C. The redistribution of photogenerated electrons near Al electrode should determine the hole tunnelling injection due to different band bending degree that depends on the number of trapped electrons in $PC_{71}BM$ near Al electrode. Therefore, electron accumulation in $PC_{71}BM$ near Al electrode may be the underlying reason for the more obvious increase of EQE values in zone B along with the increase of reverse bias.

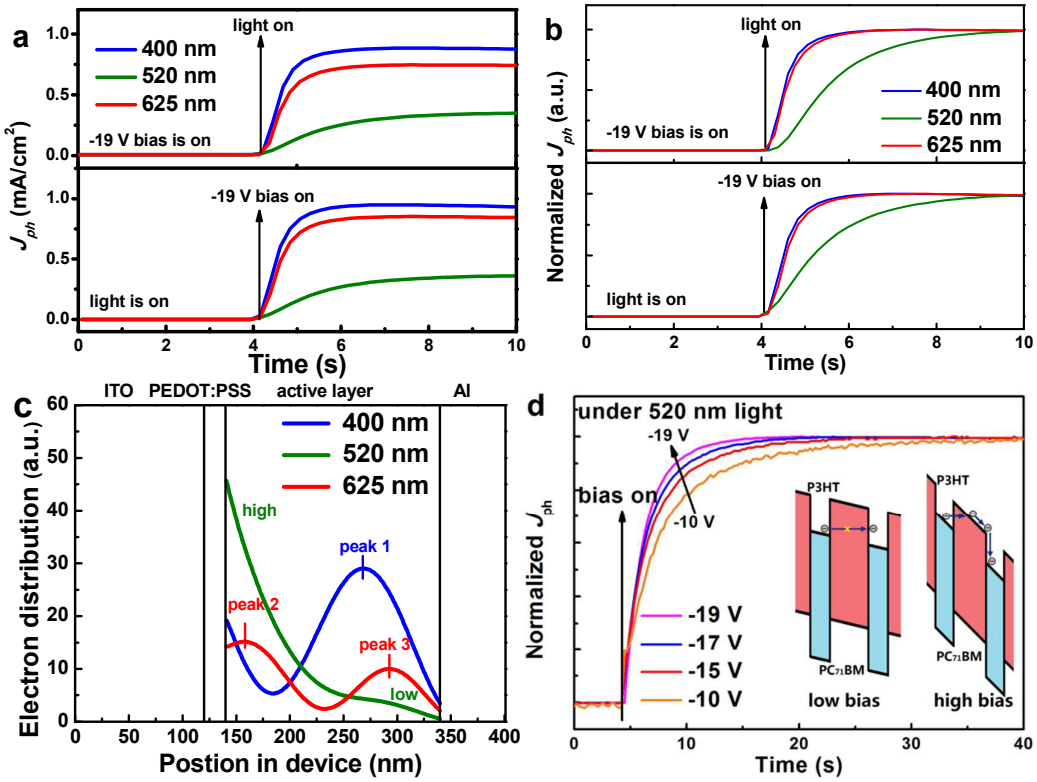

Fig. 3. (a) Transient J_{ph} curves of the PPDs measured under 400 nm, 520 nm or 625 nm light illumination and under different operation processes: i) turn-on -19 V bias and then turn-on the light; ii) turn-on the light and then turn-on the -19 V bias. (b) Normalized transient J_{ph} curves of the PPDs. (c) The normalized calculated electron distribution in PPDs under 400 nm, 520 nm and 625 nm light illumination (under zero bias). (d) The normalized transient J_{ph} curves under different biases for the PPDs under 520 nm light illumination, the insert is schematic image of electron transport under low and high bias.

It can be envisaged that electron transport should be rather weak due to the absence of electron transport channel in the P3HT:PC$_{71}$BM (100:1) films, resulting in a rather slow electron accumulation toward PC$_{71}$BM near the Al electrode under reverse bias. The rather slow electron accumulation process can be revealed by transient J_{ph} characteristics of the PPDs. The transient J_{ph} characteristics of all PPDs were measured under different light illumination and different measurement methods (turn-on light and then turn-on bias, or turn-on bias and then turn-on light), as shown in **Fig. 3a.** It is apparent that the saturated J_{ph} of PPDs under 400 nm and 625 nm light illumination are much larger than that under 520 nm light illumination, which well accords with the EQE spectra of PPDs. For turn-on bias and then turn-on light measurement method, the rise process of J_{ph} should be co-determined by the photon-electron conversion process and the electron accumulation process in PC$_{71}$BM near Al electrode. For turn-on light more than 4 seconds and then turn-on bias measurement method, the rise process of J_{ph} should be only determined by the electron accumulation process in PC$_{71}$BM near Al electrode. The number of photogenerated electrons in PC$_{71}$BM near Al electrode has arrived to a saturation state (dynamic balance) before turn-on bias, because the photon-electron conversion process is ultrafast (in about 100 fs), which has been fully confirmed by reported investigation of organic solar cells.[36] It can be seen that no matter which measurement method was carried out, the transient J_{ph} curves are almost coincident under the same wavelength light illumination. It means that the rise process of J_{ph} is mainly determined by the process of electron accumulation in PC$_{71}$BM near the Al electrode. To further confirm our speculation, the normalized transient J_{ph} curves of PPDs under different wavelength light illumination are shown in **Fig. 3b**. It is apparent that the J_{ph} of PPDs under 520 nm light illumination will take more time to arrive to its saturation state under the same reverse bias, which should be due to the initial distribution of photogenerated electrons in the active layer and the slow electron accumulation process in PC$_{71}$BM near Al electrode under reverse bias. The initial distribution of photogenerated electrons at the specific wavelengths (400 nm, 520 nm and 625 nm) is shown in **Fig. 3c** (as the cross sections marked in **Fig. 2c**)**.** It is apparent that more photogenerated electrons are generated near ITO electrode under 520 nm light illumination due to high photon harvesting ability for P3HT at this wavelength, those photogenerated electrons are rather difficult to be accumulated in PC$_{71}$BM near Al electrode due to the long

transport distance. Thus, it will take more time to accumulate photogenerated electrons in $PC_{71}BM$ near Al electrode under reverse bias, which well supports the relatively slow rise process of J_{ph} under 520 nm light illumination. For the PPDs under 400 nm or 625 nm light illumination, many photogenerated electrons have already been trapped in $PC_{71}BM$ far from ITO electrode according to the peak position in the distribution of photogenerated electrons in the active layer (as marked in **Fig. 3c**). Those electrons will be easily accumulated in $PC_{71}BM$ near Al electrode under the reverse bias due to the short transport distance, resulting in a relatively rapid rise process of J_{ph} under 400 nm or 625 nm light illumination.

According to the distribution of photogenerated electrons in the active layers, the effect of electron accumulation process on the J_{ph} rise process should be more obvious under 520 nm light illumination. The transient J_{ph} curves were measured under different reverse biases for the PPDs under 520 nm light illumination, as shown in **Fig. 3d**. It is apparent that the J_{ph} of PPDs rapidly arrives to its saturated state under higher reverse bias due to faster accumulation of photogenerated electrons in $PC_{71}BM$ near Al electrode. In fact, photogenerated electrons should overcome the different tunneling barriers to accumulate in $PC_{71}BM$ near Al electrode under different reverse biases, as shown in the insert of **Fig. 3d**. Under relatively low reverse bias, photogenerated electrons are difficult to be directly transferred from one trap (small $PC_{71}BM$ aggregation) to another trap (small $PC_{71}BM$ aggregation) by tunneling the rectangular barrier formed by P3HT. Under relatively high reverse bias, photogenerated electrons can be more easily transported from one trap to another trap by tunneling a triangular barrier formed by P3HT due to the more tilted energy levels of P3HT. Therefore, the slow J_{ph} rise process is mainly determined by the slow accumulation process of photogenerated electrons in $PC_{71}BM$ near Al electrode under different biases.

To further confirm our understanding on the effects of the initial distribution and the redistribution of photogenerated electrons on the performance of PPDs, confirmatory devices with structure of Al(1)/active layer/Al(2) were fabricated on glass substrates. The P3HT:$PC_{71}BM$ (100:1 wt %) blend films were used as the active layers for the confirmatory device. The thickness of Al(1) layer is about 20 nm to guarantee the functions as both electrode and incident light window. We define Al(1) as anode and Al(2) as cathode to accurately describe the direction of applied field. For the confirmatory devices, the hole injection barrier from Al onto the HOMO level of P3HT should be the same under forward or reverse bias. Therefore, the EQE values for the PM type PPDs under forward or reverse bias should be only determined by the number of trapped electrons in $PC_{71}BM$ near Al(1) or Al(2) electrode. The EQE spectra of confirmatory devices were measured under different reverse biases, as shown in **Fig. S2a**. The EQE spectral shapes of confirmatory devices under different reverse biases are very similar to that of PPDs, however the EQE values are much lower than those of PPDs under the same reverse bias due to the relatively low light transmittance of Al(1) layer (**Fig. S2b**). The EQE spectra of

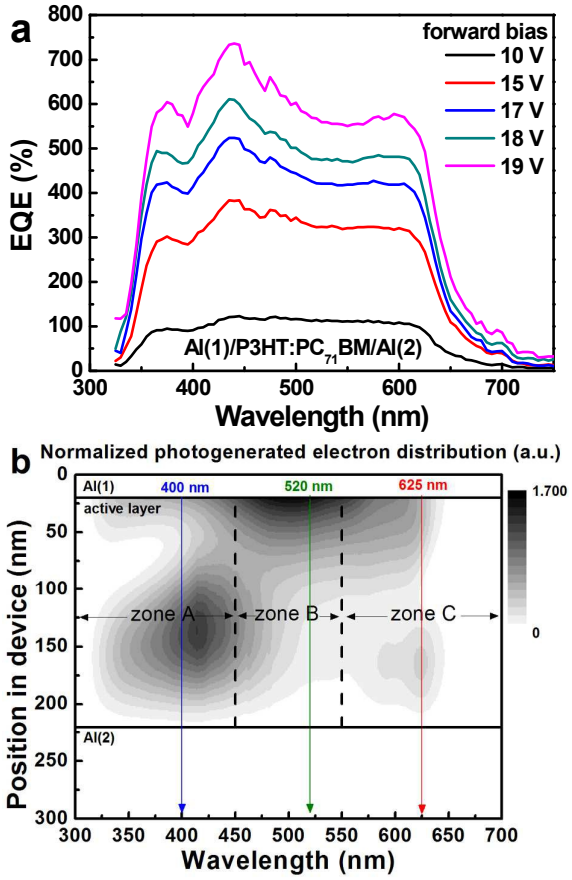

Fig. 4. (a) EQE spectra of confirmatory devices under different forward biases; (b) the calculated distribution of photogenerated electrons in the active layer of confirmatory devices (without bias).

confirmatory devices under different forward biases are shown in **Fig. 4a**. No obvious dips can be observed from the EQE spectra of confirmatory devices under forward bias. The EQE values of the confirmatory devices are much higher than 100% under reverse or forward bias. Meanwhile, the confirmatory devices exhibit significantly different EQE spectral shapes under forward or reverse bias, which should be attributed to the different distribution of photogenerated electrons near Al(1) or Al(2) under forward or reverse bias. Here, we focus on the confirmatory devices' EQE spectra dependence on the forward bias to further investigate the effects of the initial distribution and the redistribution of photogenerated electrons on the EQE spectral shape and J_{ph} rise process of PM type PPDs.

Under forward bias, holes will be injected from Al(1) electrode assisted by trapped electrons in $PC_{71}BM$ near Al(1) electrode. Therefore, the EQE spectral shape of confirmatory devices is determined by the electron distribution near Al(1) electrode under forward bias. The initial distribution of photogenerated electrons in the active layer of confirmatory devices (without bias) is calculated and shown in **Fig. 4b**. It is apparent that most of photogenerated electrons are directly trapped in $PC_{71}BM$ near Al(1) electrode once

they are generated, and the trapped electrons in $PC_{71}BM$ near Al(2) can be negligible in zone B. However, many photogenerated electrons are trapped in $PC_{71}BM$ near Al(2) electrode in zone A and zone C. It is known that the photogenerated electrons in active layer will transport toward Al(1) or Al(2) electrode under forward or reverse bias, resulting in the different electron redistribution in the active layer, especially in the $PC_{71}BM$ near electrode. Interestingly, EQE values in zone B are not higher than those in zone A and zone C under forward bias, although most of electrons are generated near Al(1) electrode in zone B. It is because the photogenerated electrons in zone B are so near Al(1) electrode that they can be very easily collected by Al(1) electrode under forward bias. The photogenerated electrons collected by Al(1) electrode will not contribute to the EQE of confirmatory devices. Moreover, the relative EQE peaks in zone A and zone C become more obvious along with the increase of forward bias due to the electron transport toward $PC_{71}BM$ near Al(1) electrode in zone A and zone C. The redistribution of electrons in $PC_{71}BM$ near electrode strongly influences hole tunneling injection from the corresponding electrode.

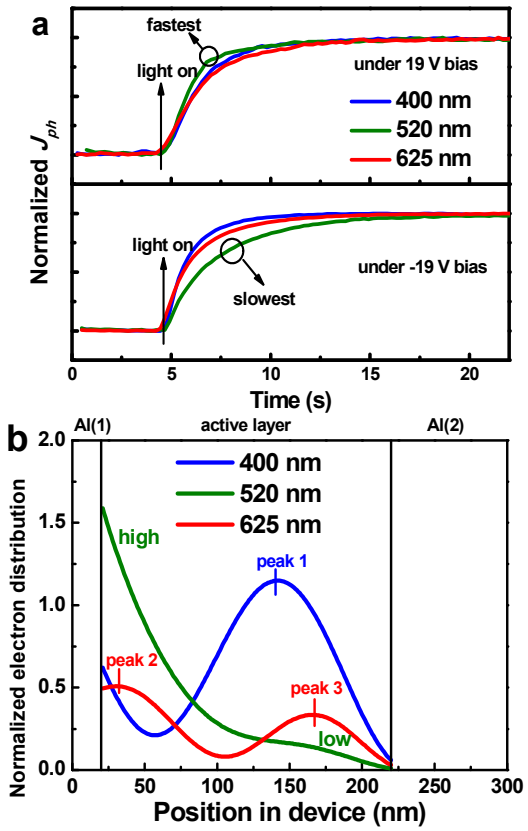

Fig. 5. (a) Normalized transient J_{ph} of the confirmatory devices under 400 nm, 520 nm or 625 nm light illumination and 19 V or -19 V bias. (b) The initial electron distribution in the confirmatory devices under 400 nm, 520 nm and 625 nm light illumination (without bias).

To further confirm the effects of the distribution and accumulation of photogenerated electrons on J_{ph} rise process of the confirmatory devices, the transient J_{ph} curves of confirmatory devices were measured under different wavelengths and biases conditions as shown in **Fig. S3**. The normalized transient J_{ph} curves of confirmatory devices are shown in **Fig. 5a**. It is apparent that the J_{ph} of confirmatory devices under 520 nm light illumination exhibits the fastest rise process under forward bias and the slowest rise process under reverse bias. The different J_{ph} rise processes can be well explained by the redistribution of photogenerated electrons in the active layer induced by electron accumulation process under bias. The initial distribution of photogenerated electrons under different wavelength light illumination was calculated according to the optical field distribution, as shown in **Fig. 5b**. It is apparent that most of electrons generated from 520 nm light illumination should be trapped in $PC_{71}BM$ near Al(1) electrode. Therefore, these photogenerated electrons will take different time to be accumulated in $PC_{71}BM$ near Al(1) or Al(2) under forward or reverse bias, resulting in the distinguished J_{ph} rise processes, respectively. When the confirmatory devices were illuminated at 400 nm or 625 nm light, the J_{ph} rise processes under forward or revere bias are relatively similar due to the relatively analogous distribution of photogenerated electrons and electron accumulation process.

In order to better understand the electron transport in the active layers of the PM type PPDs, schematic diagrams of energy level structure for PPDs under reverse bias and different conditions are shown in **Fig. 6**. When the PPDs are in dark condition, holes can hardly be tunneling injected from Al electrode to the HOMO of P3HT due to the relatively high triangular barrier, as marked in the **Fig. 6a**. When the incident light is just turned on, the most of photogenerated electrons are generated near ITO side and then trapped in $PC_{71}BM$ near ITO side, as shown in **Fig. 6b**. This initial

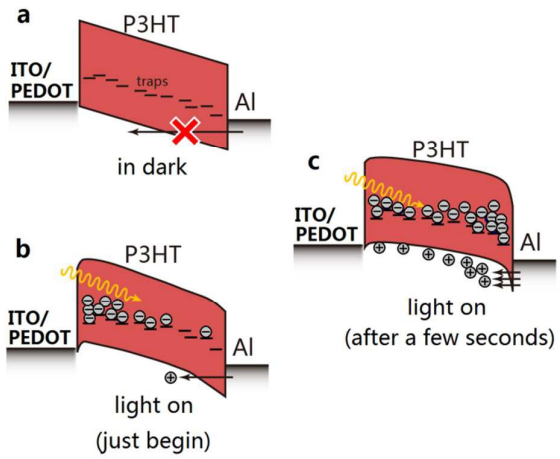

Fig. 6. Schematic diagrams of energy level structure for PPDs under reverse bias and different conditions. (a) in dark condition, (b) light illumination just begins, (c) under light illumination for a few seconds.

electron distribution can be effectively demonstrated from **Fig. 2c** and **3c**. When most of photogenerated electrons are accumulated near ITO side, the interfacial band bending near the Al electrode cannot be induced for efficient hole tunneling injection. As we can envisage, the photogenerated electrons will be transported from ITO side to Al side under reverse bias. There are two kinds of possibility for the photogenerated electrons arriving near Al electrode under reverse bias, one is trapped by $PC_{71}BM$ near Al electrode, the other is collected by Al electrode. The photogenerated electrons collected by Al electrode have no function on the trap-assisted hole tunneling injection. Only the trapped electrons in $PC_{71}BM$ near Al electrode can result in the interfacial band bending, which is beneficial to hole tunneling injection from Al electrode onto the HOMO of P3HT. After a few seconds illumination, the number of trapped electrons in $PC_{71}BM$ near Al electrode is greatly increased, resulting in a rather narrow hole tunneling injection barrier and enhanced hole tunneling injection, as shown in **Fig. 6c**. According to the energy levels of used materials, holes are easily injected onto the HOMO level of P3HT due the relatively small 0.9 eV injection barrier and hardly injected onto the HOMO level of $PC_{71}BM$ due to the relatively large 1.7 eV interfacial barrier. If the injected holes prefer to recombine with trapped electrons in $PC_{71}BM$, the trap-assisted hole tunneling injection will be decreased resulting in the disappearance of PM phenomenon. Therefore, the recombination between injected holes and trapped electrons in $PC_{71}BM$ should be very limited due the rather low $PC_{71}BM$ content in the active layers. The distribution, transport and accumulation of photogenerated electrons in the active layers co-determine the EQE spectral shape and response speed under different wavelength light illumination or applied reverse bias. Based on the above discussion and recently published paper,[37] the EQE of our reported PM type PPDS are determined by hole tunneling injection from Al electrode onto the HOMO of P3HT and hole transport along the channels formed by P3HT. The EQE of PM type PPDs was markedly increased by adjusting P3HT molecular arrangement from "edge-on" to "face-on" models which was realized by controlling the self-assembly time of P3HT:$PC_{71}BM$ active layers before annealing treatment. According to the this work and our previously published papers in this year[26, 27, 37], the working mechanism of this PM type PPDs should be clearly revealed: i) photon harvesting by P3HT; ii) rather small part exciton (close to $PC_{71}BM$) dissociated into charge carriers, electrons trapped in $PC_{71}BM$ and hole transport along P3HT channels; iii) electrons accumulated in $PC_{71}BM$ near Al electrode, resulting in interfacial band bending for the better hole tunneling injection; iv) the injected holes transport in the active layers under the reverse bias; v) injected holes collected by ITO electrode. As long as the photogenerated electrons can be trapped in $PC_{71}BM$ near Al electrode, holes can be continuously injected from external circuit and transported to ITO electrode. This is why the EQE of PM type PPDs can be much larger than unit, which provides a great potential application because a pre-amplifier circuit is not necessary for the PM type PPDs. It is kept in mind that the response speed of PM type PPDs should be further increased even up to millisecond scale for satisfying specific needs. Very recently, we have successfully reported the highly sensitive PM type PPDs with a broad spectral response range from UV light to the near infrared region[38]. The spectral response range of the PPDs can be extended to the near infrared region by doping narrow band gap polymer PTB7-Th into P3HT:$PC_{71}BM$ as the active layer. The highest EQE values of the PPDs with P3HT:PTB7-Th:$PC_{71}BM$ (50:50:1) as the active layers are around 38,000% in the spectral range from 625 nm to 750 nm under -25 V bias[38]. It means that our reported PM type PPDs may provide a new platform to obtain broad or adjusted spectral response range PM type polymer photodetectors.

Conclusions

In summary, ultrasensitive PPDs with distinct PM phenomenon were obtained based on P3HT:$PC_{71}BM$ (100:1 wt %) as the active layers. The stable champion EQE value of PPDs was ~12,600% under -19 V bias for the devices with 2,000s burn-in treatment. The PM phenomenon is attributed to the enhanced hole tunneling injection assisted by photogenerated electrons trapped in $PC_{71}BM$ near Al electrode. The EQE spectral shape and response speed of PPDs strongly depends on the bias, which can be well explained by the initial distribution of photogenerated electrons in the active layer and redistribution of photogenerated electrons under different biases. This speculation is well demonstrated by the transient J_{ph} characteristics and EQE spectra of PPDs and confirmatory devices under forward and reverse bias. This discovery may provide a new insight to increase the response speed of PM type PPDs by adjusting the photogenerated electron distribution in the active layer. Considering that the PM type PPDs have much higher EQE than the traditional organic photodetectors, the improvement may further extend its potential application with the low cost because a pre-amplifier circuit is not necessary for the PM type PPDs.

Acknowledgements

This work was supported by Fundamental Research Funds for the Central Universities (2015YJS176), National Natural Science Foundation of China (61377029), and Beijing Natural Science Foundation (2122050). J. Huang thanks the supporting from National Science Foundation under award CMM-1265834. Zhang also thanks the support from the one hundred talents project of Beijing Jiaotong University.

Notes and references

1. H. Dong, H. Zhu, Q. Meng, X. Gong and W. Hu, *Chem. Soc. Rev.*, 2012, **41**, 1754-1808.
2. A. Armin, R. D. Jansen-van Vuuren, N. Kopidakis, P. L. Burn and P. Meredith, *Nat. Commun.*, 2015, **6**, 6343.
3. R. D. Jansen-van Vuuren, A. Pivrikas, A. K. Pandey and P. L. Burn, *J. Mater. Chem. C*, 2013, **1**, 3532-3543.

4. K. H. Lee, D. S. Leem, J. S. Castrucci, K. B. Park, X. Bulliard, K. S. Kim, Y. W. Jin, S. Lee, T. P. Bender and S. Y. Park, *ACS Appl. Mater. Interfaces*, 2013, **5**, 13089-13095.
5. H. Lee, S. Nam, H. Kwon, S. Lee, J. Kim, W. Lee, C. Lee, J. Jeong, H. Kim, T. J. Shin and Y. Kim, *J. Mater. Chem. C*, 2015, **3**, 1513-1520.
6. E. Saracco, B. Bouthinon, J. M. Verilhac, C. Celle, N. Chevalier, D. Mariolle, O. Dhez and J. P. Simonato, *Adv. Mater.*, 2013, **25**, 6534-6538.
7. J. Qi, L. Ni, D. Z. Yang, X. K. Zhou, W. Q. Qiao, M. Li, D. G. Ma and Z. Y. Wang, *J. Mater. Chem. C*, 2014, **2**, 2431-2438.
8. X. Gong, M. Tong, Y. Xia, W. Cai, J. S. Moon, Y. Cao, G. Yu, C.-L. Shieh, B. Nilsson and A. J. Heeger, *Science*, 2009, **325**, 1665-1667.
9. D. Baierl, L. Pancheri, M. Schmidt, D. Stoppa, G.-F. Dalla Betta, G. Scarpa and P. Lugli, *Nat. Commun.*, 2012, **3**, 1175.
10. B. Arredondo, B. Romero, J. Pena, A. Fernández-Pacheco, E. Alonso, R. Vergaz and C. de Dios, *Sensors*, 2013, **13**, 12266-12276.
11. Z. Su, F. Hou, X. Wang, Y. Gao, F. Jin, G. Zhang, Y. Li, L. Zhang, B. Chu and W. Li, *ACS Appl. Mater. Interfaces*, 2015, **7**, 2529-2534.
12. T. Rauch, M. Boberl, S. F. Tedde, J. Furst, M. V. Kovalenko, G. N. Hesser, U. Lemmer, W. Heiss and O. Hayden, *Nat. Photonics*, 2009, **3**, 332-336.
13. H. Park, Y.-H. Kuo, A. W. Fang, R. Jones, O. Cohen, M. J. Paniccia and J. E. Bowers, *Opt. Express*, 2007, **15**, 13539-13546.
14. T. Zhai, L. Li, Y. Ma, M. Liao, X. Wang, X. Fang, J. Yao, Y. Bando and D. Golberg, *Chem. Soc. Rev.*, 2011, **40**, 2986-3004.
15. T. Kyu An, C. Eon Park and D. Sung Chung, *Appl. Phys. Lett.*, 2013, **102**, 193306.
16. R. Dong, C. Bi, Q. Dong, F. Guo, Y. Yuan, Y. Fang, Z. Xiao and J. Huang, *Adv. Opt. Mater.*, 2014, **2**, 549-554.
17. R. Saran, V. Stolojan and R. J. Curry, *Sci. Rep.*, 2014, **4**, 5041.
18. S. H. Wu, W. L. Li, B. Chu, Z. S. Su, F. Zhang and C. S. Lee, *Appl. Phys. Lett.*, 2011, **99**, 023305.
19. B. T. Lim, I. Kang, C. M. Kim, S. Y. Kim, S.-K. Kwon, Y.-H. Kim and D. S. Chung, *Org. Electron.*, 2014, **15**, 1856-1861.
20. Z. W. Jin and J. Z. Wang, *Sci Rep*, 2014, **4**, 5331.
21. H. H. Xu, J. Li, B. H. K. Leung, C. C. Y. Poon, B. S. Ong, Y. T. Zhang and N. Zhao, *Nanoscale*, 2013, **5**, 11850-11855.
22. W. T. Hammond, J. P. Mudrick and J. Xue, *J. Appl. Phys.*, 2014, **116**, 214501.
23. S.-T. Chuang, S.-C. Chien and F.-C. Chen, *Appl. Phys. Lett.*, 2012, **100**, 013309.
24. H. Y. Chen, M. K. F. Lo, G. W. Yang, H. G. Monbouquette and Y. Yang, *Nat Nanotechnol*, 2008, **3**, 543-547.
25. F. W. Guo, B. Yang, Y. B. Yuan, Z. G. Xiao, Q. F. Dong, Y. Bi and J. S. Huang, *Nat Nanotechnol*, 2012, **7**, 798-802.
26. L. L. Li, F.J. Zhang, J. Wang, Q. S. An, Q. Q. Sun, W. B. Wang, J. Zhang and F. Teng, *Sci. Rep.*, 2015, **5**, 9181.
27. L. L. Li, F. J. Zhang, W. B. Wang, Q. S. An, J. Wang, Q. Q. Sun and M. Zhang, *ACS Appl. Mater. Interfaces*, 2015, **7**, 5890-5897.
28. Q. S. An, F.J. Zhang, L. L. Li, J. Wang, Q. Q. Sun, J. Zhang, W. H. Tang and Z. B. Deng, *ACS Appl. Mater. Interfaces*, 2015, **7**, 3691-3698.
29. Q. S. An, F. J. Zhang, L. L. Li, J. Wang, J. Zhang, L. Zhou and W. H. Tang, *ACS Appl. Mater. Interfaces*, 2014, **6**, 6537-6544.
30. Q. S. An, F. J. Zhang, J. Zhang, W. H. Tang, Z. Wang, L. L. Li, Z. Xu, F. Teng and Y. S. Wang, *Sol. Energy Mater. Sol. Cells*, 2013, **118**, 30-35.
31. G. Konstantatos and E. H. Sargent, *Nat. Nanotechnol.*, 2010, **5**, 391-400.
32. L. A. A. Pettersson, L. S. Roman and O. Inganäs, *J. Appl. Phys.*, 1999, **86**, 487-496.
33. W. Li, D. Li, G. Dong, L. Duan and L. Wang, *Org. Electron.*, 2014, **15**, 3231-3236.
34. B. A. Collins, J. R. Tumbleston and H. Ade, *J. Phys. Chem. Lett.*, 2011, **2**, 3135-3145.
35. N. D. Treat, M. A. Brady, G. Smith, M. F. Toney, E. J. Kramer, C. J. Hawker and M. L. Chabinyc, *Adv. Energy Mater.*, 2011, **1**, 82-89.
36. C. J. Brabec, N. S. Sariciftci and J. C. Hummelen, *Adv. Funct. Mater.*, 2001, **11**, 15-26.
37. W. B. Wang, F. J. Zhang, L. L. Li, M. L. Gao and B. Hu, *ACS Appl. Mater. Interfaces*, 2015. In press, DOI: 10.1021/acsami.5b07522
38. W. B. Wang, F. J. Zhang, L. L. Li, M. Zhang, Q. S. An, J. Wang and Q. Q. Sun, J. Mater. Chem. C, 2015, **3**, 7386-7393